Integrated Computational and Experimental Protocol for Understanding Rh(III) Speciation in Hydrochloric and Nitric Acid Solutions

ARTICLE *in* INORGANIC CHEMISTRY · NOVEMBER 2014

Impact Factor: 4.76 · DOI: 10.1021/ic501408r · Source: PubMed

6 AUTHORS, INCLUDING:

Alex Samuels
Washington State University
7 PUBLICATIONS **4** CITATIONS
SEE PROFILE

Sue Clark
Washington State University
43 PUBLICATIONS **556** CITATIONS
SEE PROFILE

Nathalie A Wall
Washington State University
42 PUBLICATIONS **252** CITATIONS
SEE PROFILE

Aurora E Clark
Washington State University
80 PUBLICATIONS **1,292** CITATIONS
SEE PROFILE

Inorganic Chemistry

Article

pubs.acs.org/IC

Integrated Computational and Experimental Protocol for Understanding Rh(III) Speciation in Hydrochloric and Nitric Acid Solutions

Alex C. Samuels,[†,‡] Cherilynn A. Boele,[†] Kevin T. Bennett,[†] Sue B. Clark,[†] Nathalie A. Wall,*[,†,‡] and Aurora E. Clark*[,†,‡]

[†]Department of Chemistry, Washington State University, Pullman, Washington 99164, United States,

[‡]Materials Science and Engineering Program, Washington State University, Pullman, Washington 99164, United States

Supporting Information

ABSTRACT: Platinum group metals (PGMs), including rhodium, generated by the fission of ^{235}U are present in significant quantities within spent nuclear fuel located on power generation sites in the United States, the amount of which is expected to exceed natural reserves by 2030. Yet, spent fuel raffinates are highly acidic media that may result in complex speciation of the PGM. This work provides an understanding of Rh(III) speciation up to 9 M HCl and HNO_3, and utilizes a combination of ultraviolet−visible (UV-vis) and capillary zone electrophoresis data, along with computationally predicted thermochemistry and simulated UV-vis spectra to approximate the relative concentrations of potential species in solution as a function of acid concentration. One Rh(III) species, $[Rh(NO_3)_3]$, is observed under all conditions in HNO_3 and for Rh(III) concentrations smaller than 10^{-3} M. In contrast, a variety of chloridated Rh(III) species may exist simultaneously in a HCl medium. The species $[RhCl_2(H_2O)_4]^+$ and $[RhCl_3(H_2O)_3]$ are observed in HCl solutions of concentrations ranging from 0 to 1 M; the species $[RhCl_4(H_2O)_2]^-$, $[RhCl_5(H_2O)]^{2-}$, and $[Rh_2Cl_9]^{3-}$ are observed between 2 and 9 M HCl.

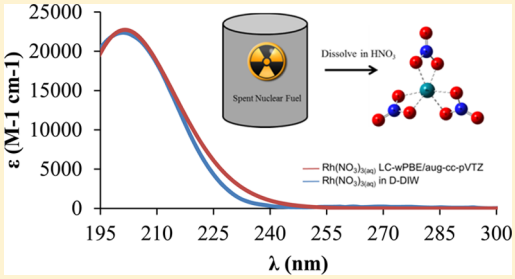

1. INTRODUCTION

Studies of Rh speciation in acidic solutions received significant interest in the 1960s and 1970s, motivated, in part, by precious metal refining and in part due to complex and interesting solution-phase chemistry. The separation of Rh from other platinum group metals (PGMs) continues to be relevant to modern separations chemistry, as natural deposits become depleted and spent nuclear fuel (SNF) is being considered a potential feedstock.[1,2] Rhodium, as well other PGMs are produced by ^{235}U fission, yielding ∼4 kg of PGMs per ton of waste for a commercial light water reactor (PWR fuel, 32.3 GW d t^{-1}; 880 d irradiation; 3.2% ^{235}U as UO_2; fluence, $F = 3.24 \times 10^{14}$ n cm^{-2} s^{-1}) .[3] It is estimated that by the year 2030, the amount of fission-generated Rh could exceed known natural reserves.[3] The only stable Rh isotope, ^{103}Rh, is obtained directly as a fission product; it is also produced by β^- decay of the fission product, ^{103}Ru ($t_{1/2}$ = 40 d).[4] Thus, upon proper separations and after cooling time for at least 50 years, Rh extracted from spent nuclear fuel could be used for industrial purposes.[5]

Raffinates from extraction processes that remove heavier lanthanide and actinides from SNF typically leave the PGMs at near room temperature in aqueous acidic solutions containing chloride or nitrate.[6] The pH is generally <1, with moderate to concentrated chloride concentrations (up to 6 mol L^{-1} (M)), and nitrate concentrations of 2−4 M.[6,7] Rh is quite stable in the trivalent oxidation state; however, the speciation kinetics in chloride media is particularly complicated. The completely aquated hexa-aquarhodium(III), $[Rh(H_2O)_6]^{3+}$, the hexachloridorhodate(III), $[RhCl_6]^{3-}$, and all mixed aqua/chlorido complexes, including isomers, $([RhCl_x(H_2O)_{6-x}]^{3-x}$ with x = 1−5) can exist simultaneously in solution. At high chloride concentrations and millimolar Rh(III) concentrations, a dimer, $[Rh_2Cl_9]^{3-}$, has been reported to form.[8] Further adding to the variety of complexes possibly present are chloride and oxygen-bridged polymeric Rh species, of which very little is known.[9] The formation of polymeric species is not unique to Rh(III) and is observed with Cr(III) and Fe(III), at pH <7 and metal concentrations of $\geq 10^{-3}$ M.[10,11] The concentration of each complex depends primarily on the chloride concentration, but also, to a lesser degree, on the temperature, age, and pH of the solution. For example, at pH >2.9, the aqua/chlorido complexes are believed to undergo hydrolysis to form $[RhCl_4(OH)(H_2O)]^{2-}$.[12] As a result of the complicated species distribution in solution, study of the chlorido-aqua species has relied upon purification of a specific species of interest via ion exchange chromatography, followed by characterization using polarography and/or ultraviolet−visible (UV-vis) spectroscopy (focusing upon the low-energy portion of the spectrum, $\lambda \geq$ 300 nm). Significant efforts have been devoted to understanding the mechanistic aspects of aquation reactions of

Received: June 18, 2014
Published: November 12, 2014

   dx.doi.org/10.1021/ic501408r | Inorg. Chem. 2014, 53, 12315−12322

Table 1. Concentrations of Rh Used for Data Collection (after Dilution) of the UV-vis Spectrum, as a Function of Acid Concentration Employed during Equilibration after the Addition of HCl or HNO_3

	Rh Concentration [M]	
acid concentration during equilibration	during $\lambda_{UV\text{-}vis}$ (190−600 nm)	during $\lambda_{UV\text{-}vis}$ (300−800 nm)
0.0	9.2 (±0.1) × 10^{-6} (HCl)	9.2 (±0.1) × 10^{-4} (HCl)
	2.69 (±0.06) × 10^{-5} (HNO_3)	
0.1	1.09 (±0.03) × 10^{-5} (HCl)	1.09 (±0.03) × 10^{-3} (HCl)
0.5	1.05 (±0.02) × 10^{-5} (HCl)	1.05 (±0.02) × 10^{-3} (HCl)
1.0	1.03 (±0.06) × 10^{-5} (HCl)	1.03 (±0.06) × 10^{-3} (HCl)
2.0	9.9 (±0.3) × 10^{-6} (HCl)	9.9 (±0.3) × 10^{-4} (HCl)
	5.36 (±0.05) × 10^{-5} (HNO_3)	
4.0	2.73 (±0.06) × 10^{-5} (HNO_3)	
6.0	9 (±1) × 10^{-6} (HCl)	9 (±1) × 10^{-4} (HCl)
	2.73 (±0.05) × 10^{-5} (HNO_3)	
8.0	9.4 (±0.6) × 10^{-6} (HCl)	9.4 (±0.6) × 10^{-4} (HCl)
	5.36 (±0.07) × 10^{-5} (HNO_3)	
9.0	1.1 (±0.1) × 10^{-5} (HCl)	1.1 (±0.1) × 10^{-3} (HCl)
10.0	5.22 (±0.05) × 10^{-5} (HNO_3)	
12.0	2.99 (±0.05) × 10^{-5} (HNO_3)	

various chlorido-aqua species.[13−17] In principle, speciation under varying chloride concentrations should be straightforward to determine provided the binding constants of all potential molecular species; however, the available speciation diagrams are suspect as different interpretations of the polarographic data yield a range of binding constants. Even less is understood about the speciation of Rh(III) in nitric acid media, as nucleophilic substitution of chloride by nitrate has been observed.[18]

Examination of Rh speciation under conditions relevant to extraction from raffinates is necessary to design extraction protocols for this metal from spent fuel. To aid in the assignment of species within solution and to understand the potentially intricate distribution and dynamic nature of species, modern studies can take advantage of computational chemistry to understand the thermodynamic favorability for the formation as well as the prediction of the UV-vis spectra of individual entities. The goal of this work is 2-fold: first, to investigate Rh(III) speciation in acidic media under conditions that are relevant to separations applied to spent fuel raffinates, and second, to demonstrate that the speciation can be understood through a combined experimental and theoretical approach that relies upon identification of the number of species present using electrophoretic methods, experimental measurement of ligand−metal charge transfer (LMCT) bands in the UV-vis region, simulation of the UV-vis spectra, and calculated thermodynamic quantities. The speciation of Rh(III) nitrate is shown to be straightforward; however, Rh(III) chloride speciation in acidic aqueous solutions is significantly more complex than prior work indicates.

2. EXPERIMENTAL SECTION

Materials and Methods. Samples presumed to be $RhCl_3 \cdot nH_2O$ (99.99% Rh purity, Fisher) were dissolved in deionized distilled 18 MΩ water (D-DIW), under constant stirring at room temperature, except for daily low heating (1 h/day), until equilibrium was reached. Solutions were protected from light at all times. The Rh chloride speciation was perturbed by adding aliquots of $RhCl_3$ stock solutions, described above, to D-DIW and enough 12 M HCl (Fisher) to obtain various chloride concentrations (Table 1). The resulting solutions were stirred for 1 min before being placed in a 50 °C oven, where they remained until solutions reached equilibrium. During this time, the solutions were stirred for 1 min daily and momentarily removed from the oven at recorded times for UV-vis analysis (the solutions were allowed to cool before measurements). Sodium (Na) concentrations in the $RhCl_3$ solutions in water were determined using an atomic absorption flame emission spectrophotometer (Flame AA) (Shimadzu, Model AA-6200) (Buck Scientific Na/K Hollow Cathode Lamp, lamp current 14 V, slit width 0.2 nm, wavelength 589.0 nm). The instrument was calibrated with dilutions of a 1003 ppm of Na standard solution in 5% HNO_3 (VHG Laboratories). Rhodium nitrate solutions were prepared in a similar fashion. A solid sample presumed to be $Rh(NO_3)_3 \cdot nH_2O$ (36% Rh metal basis by weight, Sigma−Aldrich) was dissolved in D-DIW. Once dissolved, the Rh nitrate solution turned yellow. An attempt was made to prepare $[Rh(NO_3)_x]$ (with $x > 3$), by adding aliquots of $[Rh(NO_3)_3]$ to D-DIW and concentrated HNO_3 (Fisher). Rh chloride and Rh nitrate samples reached equilibrium when UV-vis spectra remained unchanged between two consecutive daily measurements.

UV-vis spectra of the Rh chloride and Rh nitrate solutions were obtained at regular time intervals (at least weekly) using a Cary Model 5000 UV-visible spectrophotometer (Varian/Agilent). Solution absorbances were measured between 300 and 800 nm for the low-energy absorption feature, and between 190 and 600 nm for the high-energy band. Rh samples were equilibrated with Rh concentrations of ca. 10^{-3} M, but subsequent UV-vis measurements required dilutions. Low-energy UV-vis measurements (λ = 300−800 nm) were performed with Rh concentrations at ca. 10^{-3} M, while high-energy absorbance (λ = 190−600 nm) required Rh concentrations of ca. 10^{-5} M (Table 1). Rh concentrations were determined by inductively coupled plasma−optical emission spectrometry (ICP-OES) (Perkin−Elmer, Model Optima 3200 RL). The instrument was calibrated using dilutions of a 1000 ppm Rh standard solution in 10% HCl (Acros Organic).

Capillary zone electrophoresis (CZE) (Agilent 7100 Capillary Electrophoresis System) was performed using the Rh solutions described in Table 1 to determine the minimum number of chloridated species and to estimate species charge. The observed number of species from CZE is considered to be the minimum number, because the molar absorptivity for each of the Rh chlorides is quite small and may not be detectable at the concentrations employed. The capillary (PolyMicro Technologies) was 60 cm long (53 cm to the detection window), with an inner diameter of 75 μm. The applied voltage spanned −30 and 30 kV to enable identification of both negative and positive species. The temperature of the capillary was held constant at 25 °C. Solutions were injected hydrodynamically at 5 mbar for 10 s. UV−vis (200−600 nm) was used for detection, in 2.0 nm increments. New capillaries were conditioned by flushing with 1.0 M KOH (5 min), D-DIW (5 min), 1.0 M HCl (5 min), D-DIW (5 min), and background electrolyte (BGE) (5 min). The preconditioning of the capillary consisted of flushing with 0.1 M KOH (5 min), D-

dx.doi.org/10.1021/ic501408r | Inorg. Chem. 2014, 53, 12315−12322

DIW (5 min), 1.0 M HCl (5 min), D-DIW (5 min), and BGE (5 min). After the final run, post-conditioning of the capillary consisted of flushing with D-DIW for 20 min. The background electrolytes that were used contained 10 mM $NaClO_4$, and various concentrations of HCl to match the concentration of the HCl of the different samples (Table 1). The pH of the BGE was adjusted to 3.7 with $HClO_4$. Acetone (1 M) was also added in some cases to identify the electroosmotic flow (EOF) band. Once the EOF was identified, the samples were run again in the absence of acetone to identify the absorption associated with Rh-containing species. Acetone that was added to some of the samples was detected at a wavelength of 280 nm and also with a contactless conductivity detector (TraceDec Contactless Conductivity Detector). OpenLAB CDS ChemStation (Agilent Technologies) was used for data analysis.

Computational Methods. The B3LYP combination of density functionals was employed for the optimization of the gas-phase hydrated Rh(III) as $[Rh(H_2O)_6]^{3+}$ and the chloride- and nitrate-substituted species $[RhCl_x(H_2O)_y]^{3-x}$ ($x = 0-6$; $y = 6 - x$), $[Rh(NO_3)_x(H_2O)_y]^{3-x}$ ($x = 0-3$; $y = 6 - 2x$), and $[Rh_2Cl_9]^{3-}$, using the NWChem software package.[19−22] The cc-pVDZ basis set was used to describe all atoms. In the case of Rh(III), this consists of segmented contracted 4s4p3d1f functions, along with a matching pseudopotential that replaces the 28 inner-shell ($[Ar]4s^23d^8$) electrons.[23−25] Frequency calculations were performed on all optimized structures to obtain thermochemical corrections and ensure that they correspond to a local minima.

Single-point conductor-polarized continuum model (CPCM) calculations were performed as implemented in the development version of Gaussian09.[26] The solvent-corrected free energies (in water) of the replacement reactions that produce the chloride and nitrate species from the hydrated ion are defined by

$$\Delta G_{rxn} = \Delta G^{298}_{gas} + \Delta G_{solv} + SS_{corr} \quad (1)$$

which has ΔG^{298}_{gas} as the free energy of the reaction in the gas-phase, ΔG_{solv} as the solvation contribution to the free energy of the reaction, and SS_{corr} as the standard-state thermodynamic correction (−4.3 kcal/mol for each $(H_2O)_n$ water cluster).[27] Geometry optimization of $[RhCl_3(H_2O)_3]$ was performed in the solution phase using CPCM as a test to ensure a similar geometry and electronic structure was obtained. Indeed, the solution-phase geometry exhibited only minimal elongation (<0.1 Å) of the Rh−Cl and Rh−OH_2 bond lengths, relative to the gas phase.

As multiple species may exist experimentally, the goal of this work is to utilize the computed oscillator strengths for the electronic transitions to simulate the experimental UV-vis spectrum in aqueous solution. A computational protocol that is easily adopted by a broader community is desired, to maximize the general applicability of a combined experimental and computational approach and to dissect the complex speciation of metal ions in solution. As such, time-dependent density functional theory (TD-DFT) was used to compute the excited-state energies and transition oscillator strengths in solution for each optimized Rh(III) species. However, it is quite difficult for a single density functional to optimally describe all of the different types of excited states in a transition-metal complex simultaneously (charge transfer vs $d-d$ transitions, for example). Thus, we have focused upon accurate reproduction of the high-energy LMCT-based electronic transitions for Rh complexes, using the long-range corrected PBE0 (LC-wPBE) functional, which has exhibited much success in predicting these types of excitations.[28,29] The basis sets for the TD-DFT calculations utilized the aug-cc-pVTZ with the corresponding pseudo-potential for Rh(III) and aug-cc-pVTZ basis sets for all other atoms.[23−25] Larger basis sets were used in the TD-DFT calculations, as opposed to geometry optimizations, as a more complete basis set yields better orbital descriptions. Several different continuum models (CPCM, IEF-PCM, and COSMO) were examined for the accurate reproduction of the UV-vis spectrum of a single species, $[Rh(NO_3)_3]$, with only CPCM being successful (*vide infra*).

To compare theoretical data with experiment, oscillator strengths for the electronic transitions calculated in Gaussian09 were converted to molar absorptivity using

$$\varepsilon_i(\tilde{\nu}) = \frac{e^2 N\sqrt{\pi}}{1000\ln(10)c^2 m_e}\left(\frac{f_i}{\sigma}\right)\exp\left[-\left(\frac{\tilde{\nu}-\tilde{\nu}_i}{\sigma}\right)^2\right] \quad (2)$$

where ε_i is the electronic excitation of interest, $e = 4.803204 \times 10^{-10}$ esu, $N = 6.02214199 \times 10^{23}$, $c = 2.997924 \times 10^{10}$ cm/s, $m_e = 9.10938 \times 10^{-31}$ g, f_i is the oscillator strength, σ is the standard deviation in wavenumbers ($\sigma = 0.5$ eV) and is related to the width of the band, and at the maximum of the band where the energy of the incident radiation ($\tilde{\nu}$) is equal to $\tilde{\nu}_i$.[30] When there are multiple electronic excitations in the spectral region of interest, the spectrum becomes a sum of all of the individual bands:

$$\varepsilon(\tilde{\nu}) = \sum_{i=1}^{n} \varepsilon_i(\tilde{\nu}) \quad (3)$$

The resulting theoretical spectra were then used to fit the experimental spectrum, based on the relative concentrations of different Rh(III) species by minimizing the normalized root-mean-squared deviation (NRMSD) between the combined theoretical spectrum and the experimental one through modification of the percent contribution of each Rh(III) chloride species. This is directly analogous to deconvoluting the experimental spectrum into subspecies experimental spectra.[14] A NRMSD of 5% was chosen as a threshold for a fit to be considered reasonable, and the combinations that yielded a NRMSD below the threshold were examined.

RESULTS AND DISCUSSION

3.1. Thermochemical and UV-vis Identification of Rh(III) Species in Nitric Acid Media. Prior to this work, the speciation of Rh in nitric acid had not been extensively studied, but it is believed to be heavily influenced on the initial Rh complex dissolved in solution.[12,18,31] X-ray diffraction (XRD) studies performed by Belyaev et al. and Caminiti et al. suggest the presence of a Rh(III) dimer in acidic solutions where the $[NO_3^-] > 1$ M and Rh concentrations of 10^{-1} M.[18,31] At lower Rh(III) concentrations, like those present in SNF, a monomeric Rh(III) nitrate species was suggested, which has been supported by UV-vis and capillary electrophoresis data obtained in acidic media by Aleksenko et al.[18]

Here, the speciation of Rh(III) in nitric acid was first examined by calculating the thermodynamic favorability of successive nitrate additions to an initial $[Rh(H_2O)_6]^{3+}$ cluster in aqueous solution (Table 2). Initial geometries presumed a bidentate coordination geometry for the nitrate, as observed previously with other transition-metal nitrate complexes.[32,33] Stable monodentate bound nitrates were pursued but no low-energy optimized structures were found, nor were any species

Table 2. Calculated Solution-Phase Free Energies of the Successive Nitrate Addition Reactions to the Initial $[Rh(H_2O)_6]^{3+}$ Species, along with the TD-DFT Calculated λ_{max} of the $Rh(NO_3)_x(H_2O)_y]^{3-x}$ ($x = 0-3$; $y = 6 - 2x$) Products between 180 nm and 800 nm

rxn	ΔG_{rxn} [kcal/mol]	λ_{max}(product) [nm]
$[Rh(H_2O)_6]^{3+}_{(aq)} + NO_3^-{}_{(aq)} \rightarrow [Rh(H_2O)_4(NO_3)\ ]^{2+}_{(aq)} + 2H_2O_{(aq)}$	−44.55	184
$[Rh(H_2O)_4(NO_3)\ ]^{2+}_{(aq)} + NO_3^-{}_{(aq)} \rightarrow [Rh(H_2O)_2(NO_3)_2]^{+}_{(aq)} + 2H_2O_{(aq)}$	−15.73	196
$[Rh(H_2O)_2(NO_3)_2]^{+}_{(aq)} + NO_3^-{}_{(aq)} \rightarrow [Rh(NO_3)_3]_{(aq)} + 2H_2O_{(aq)}$	−13.05	202

dx.doi.org/10.1021/ic501408r | *Inorg. Chem.* 2014, 53, 12315−12322

that contained four or more nitrates in the primary coordination sphere. The optimized structures exhibited an increase in the bond length r_{Rh-O_2NO} and r_{Rh-OH_2} (see Table S1 in the Supporting Information), with each subsequent nitrate replacement. Beginning with the octahedral hydrated ion, each nitrate addition is very thermodynamically favorable ($\Delta G_{rxn} \leq -44$ kcal/mol), indicating that (i) the trinitrate complex is likely to be present in aqueous solution (Table 2) and (ii) bound nitrates are unlikely to dissociate until a stronger complexant is added to solution. The theoretical spectra of the aqueous mononitrate, dinitrate, and trinitrate species of Rh(III) are predicted to have distinct peak positions in the range of 184−202 nm in the UV-vis spectrum. These absorption bands are found to be derived from LMCT transitions. Based on these calculations, different nitrate species should be clearly evident within the experimental UV-vis spectrum.

The experimental data reinforces the thermodynamic predictions of a single species of Rh(III), $[Rh(NO_3)_3]$, in nitrate media. The stock solution of 10^{-3} M Rh(III) nitrate reached equilibrium after 3 weeks of continuous stirring, during which the solution color changed from clear to yellow. A UV-vis spectrum was obtained in the 800−300 nm range to examine the low-energy transitions, where $d-d$ transitions are typically manifested. No distinct peaks were observed, indicating high symmetry structures with forbidden $d-d$ transitions. A peak below 300 nm with a molar absorptivity much larger than 1000 was observed, having a peak position of 202 nm. The samples of the stock solutions with nitrate concentration between 0 and 12 M, presented in Table 1, were continuously stirred and reached equilibrium in a week. UV-vis spectra exhibit one absorbance band in all solutions with a λ_{max} = 202 nm (molar absorptivies were within error of each other and had a value of 22 310 M^{-1} cm^{-1} (see Table S2 in the Supporting Information). Examination of the theoretical spectrum of $[Rh(NO_3)_3]$ using a Gaussian bandwidth of 0.5 eV, and eqs 2 and 3, reveal a single peak derived from LMCT and ligand $\pi-\pi^*$ transitions also centered at 202 nm. As shown in Figure 1, the $[Rh(NO_3)_3]$ theoretical spectrum has only a 3% NRMSD with the experimental spectrum of $[Rh(NO_3)_3]$ dissolved in water, with the position of the band at 202 nm, the band shape, and its absorptivity, being accurately reproduced. In combination, the theoretical and experimental data indicate that the presumed $[Rh(NO_3)_3]$ that was initially dissolved in solution is maintained in the molecular form in the aqueous phase and at varying concentration of nitric acid. Based on calculated thermodynamic data, it is further anticipated that, in other solution-phase environments, where 10^{-3} M Rh(III) is dissolved in nitric acid, once the $[Rh(NO_3)_3]$ is formed, it will be the stable kinetic and thermodynamic end product in the absence of another strong complexant. The significantly different λ_{max} values predicted for each of the $[Rh(H_2O)_4(NO_3)]^{2+}$, $[Rh(H_2O)_2(NO_3)_2]^{+}$, and $[Rh(NO_3)_3]$ species should help in species identification in future studies.

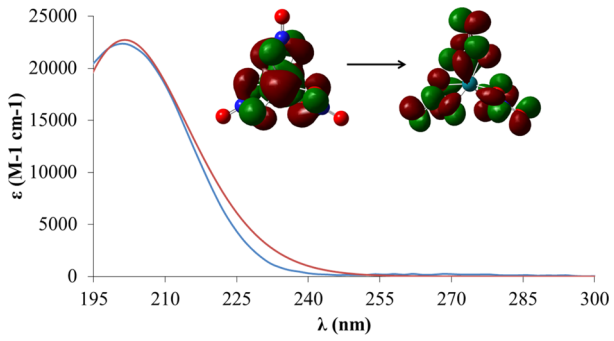

Figure 1. Experimental spectrum of $[Rh(NO_3)_3]$ ([Rh] ca. 10^{-5} M) dissolved in pure water (blue) overlaid with the LC-wPBE/aug-cc-pVTZ (red) predicted UV-vis spectrum with the primary orbitals involved in the dominant transition shown. Key structural parameters are presented in Table S1 in the Supporting Information.

3.2. Thermochemical and UV-vis Identification of Rh(III) Species in Hydrochloric Acid Media. Past studies have demonstrated that speciation of Rh(III) in hydrochloric acid is complex. Species identification has relied heavily on UV-vis spectroscopy, focusing on the absorptions between 300 and 800 nm (presumably the $d-d$ absorption bands, which have a limited allowedness due to low symmetry).[13−17,34] After separation using chromatography, a study of Wolsey et al. determined the identifying UV-vis peak positions and molar absorptivities in this range for all of the chloridated Rh(III) aqua species in solution conditions that spanned 0.1 to 2 M HCl.[13−17] Subsequent studies focused on the chloride exchange reactions in the first coordination sphere. These works have suggested that successive chloride substitution reactions of $[Rh(H_2O)_6]^{3+}$ to form $[RhCl_5(H_2O)]^{2-}$ are favorable in solution where the concentration of HCl is greater than 0.07 M. The formation of $[RhCl_6]^{3-}$ is unfavorable and is only possible at temperatures above 70 °C, as would be expected, based on the relative steric bulk of the chloride ligands, the ionic radius and electrophilicity of Rh(III).[14] Most of these studies have been performed at temperatures greater than or equal to 50 °C and in the presence of perchloric acid. Thus, the reported thermodynamic favorability of chloride substitution may be diminished under the room-temperature conditions anticipated for SNF raffinates. Importantly, the complex species distribution of Rh(III) in HCl solution has not been systematically pursued. Aleksenko et al. studied Rh(III) speciation under the two extremes of 0.1 and 11 M HCl using capillary electrophoresis to separate the species in solution, with a subsequent report of the UV-vis spectra of LMCT bands for identification of the individual species.[12] Generally, as the concentration of HCl was increased, the number of chlorides coordinated to Rh(III) increased, and a mixture of Rh chloride species was suggested at both chloride concentrations. However, Aleksenko's reported UV-vis wavelength of λ_{max} = 250 nm differs from other reports that established a stepwise shift to shorter wavelengths of all the absorbance bands on substitution of H_2O for Cl^- ligands, suggesting the presence of a complex mixture in solution. Thus, disparity exists regarding both the profile and the higher energy absorbance bands in the UV-vis spectra of individual Rh(III) chloridated species and the speciation of Rh(III) as the concentration of hydrochloric acid is increased. The results and discussion herein first describe the overall features of the TD-DFT predicted spectra of Rh(III) chloride species as the number of chloride ligands is increased, and experimental UV-vis spectra as the concentration of HCl is increased. The speciation of dissolved Rh(III) chloride then is established using data from the predicted thermodynamic properties of chloride substitution, the TD-DFT spectra, along with capillary zone electrophoresis data.

The TD-DFT UV−vis absorption spectra of $[RhCl_x(H_2O)_y]^{3-x}$ (x = 0−6; $y = 6 - x$) contain one or two distinct absorption peaks below 300 nm for each species (see

dx.doi.org/10.1021/ic501408r | Inorg. Chem. 2014, 53, 12315−12322

Figure S1 and Table S3 in the Supporting Information), with a general red shift upon the each chloride substitution. It is important to note that there are distinct differences in the predicted spectra of Rh(III) chloride species, depending on the isomer. In the case of the *cis*- and *trans*- $[RhCl_2(H_2O)_4]^+$ and $[RhCl_4(H_2O)_2]^-$, individual species have λ_{max} values that differ by ≥10 nm. This is relevant as prior separations and identification of the high-energy region of the UV-vis spectra have not distinguished contributions from different isomeric species that may be present.[35] When considering the spectra obtained from Rh(III) in a wide range of chloride concentrations, unique absorption bands are observed (see Figures S2 and S3 in the Supporting Information); however, the peak positions and shapes do not agree with the predicted spectra for a single species (Figure S1) nor the prior reported peak positions reported by Blasius or Aleksenko for isolated Rh(III) chloride species.[12,35] The experimental spectra do exhibit the anticipated red shift in the 300−800 nm absorbance peaks, which is consistent with an overall increase in chloride coordination with increased HCl (see Table 3).

Table 3. Literature UV-vis Wavelength (λ_{max}) for Individual Rh Species and UV-vis Absorption Maxima as a Function of the HCl Concentration of the Rh Chloride Solutions[a]

(a) Literature UV-vis Wavelength (λ_{max}) for Individual Rh Species

species	λ_1	λ_2	ref	λ_3	λ_4	ref
$[RhCl(H_2O)_5]^{2+}$				335	426	34
cis-$[RhCl_2(H_2O)_4]^+$	201	220	35	355	450	14
trans-$[RhCl_2(H_2O)_4]^+$				350	450	14
cis-$[RhCl_3(H_2O)_3]$	201	223	35	376	474	34
trans-$[RhCl_3(H_2O)_3]$				370	471	34
$[RhCl_4(H_2O)_2]^-$	201	223	35	385	488	34
$[RhCl_5(H_2O)]^{2-}$	201	242	35	402	507	34
$[RhCl_6]^{3-}$	207	253	35	411	518	34
$[Rh_2Cl_9]^{3-}$				414	524	8

(b) UV-vis Absorption Maxima, as a Function of the HCl Concentration of the Rh Chloride Solutions

HCl (M)	λ_1	λ_2	λ_3	ref
0.0	221	357	449	present work
0.1	225	368	465	present work
0.5	225	374	471	present work
1.0	226	385	484	present work
2.0	226	396	497	present work
6.0	249	410	511	present work
9.0	250	408	517	present work

[a]The observed λ_{max} values from Figure S1 in the Supporting Information are also presented.

Speciation of Dissolved Rh Chloride in Pure Water. The dissolution of the Rh chloride sample in D-DIW occurred within minutes, while several months were necessary to reach a metastable solution equilibrium defined by unchanging UV-vis spectra over the course of several days. This is important, as prior work has suggested that the solution composition can change for Rh(III) in HCl over the course of years. During the dissolution and equilibrium process, the solution color changed from red to yellow. The high-energy feature of the UV-vis spectrum for the 0 M HCl solution has a maximum at 221 nm, while the lower energy portion of the spectrum contains two features with maxima at 369 and 463 nm, respectively (see Table 3). Prior assignment of the low-energy absorptions of the isolated meridional isomer of aqueous $[RhCl_3(H_2O)_3]$ have wavelength maxima of 471 and 370 nm, while the facial isomer has maxima at 474 and 376 nm.[13,34]

Based on these literature data, it is apparent that a mixture of species results from dissolution of the initial sample, as the peak at 463 nm cannot arise from either the facial (*fac*) or meridional (*mer*) isomers (λ_{max} of 474 and 471 nm, respectively), or any mixture of these two species.[8,14,34] The reported *d*−*d* absorbance bands of isolated *cis*-$[RhCl_2(H_2O)_4]^+$ are located at 358 and 453 nm, while that of $[RhCl(H_2O)_5]^{2+}$ occur at 335 and 426 nm (see Table 3).[34] Thus, it is likely that some of these monochloride and dichlorido species exist in solution and are responsible for the deviations in the *d*−*d* band positions. The possibility of the Rh(III) chloride sample having impurities that may result in multiple species in the aqueous solution is confirmed by flame AA analysis, which indicates a small Na-to-Rh molar ratio in the solution of the dissolved sample prepared in D-DIW (3×10^{-3}). Consequently, it is envisioned that Na^+ was introduced in the sample as counterion to chloride and the $RhCl_3{\cdot}nH_2O$ sample maybe a mixture of $[RhCl_x(H_2O)_{x-6}]^{3-x}$ species that derive from the methodology for preparation.[36] The capillary electrophoresis data indicates the presence of a neutral species in solution; however, this value is used as a lower bound to the potential number of species present because the CZE may omit the presence of some species due to the low molar absorptivities at the concentration employed and may not resolve isomers. A linear combination of the TD-DFT spectra of the *fac* and *mer* isomers of $[RhCl_3(H_2O)_3]$ yields a fit to the LMCT portion of the experimental UV−vis spectrum having an NRMSD of 6%, beyond the threshold of acceptable tolerance for fitting (see Figure S4 in the Supporting Information). NRSMD values below 5% are obtained when the relative composition of the spectrum is 0−6% *trans*-$[RhCl_2(H_2O)_4]^+$, 48%−50% *cis*-$[RhCl_2(H_2O)_4]^+$, and 46%−50% *mer*-$[RhCl_3(H_2O)_3]$ (see Figure 2). The very best NRMSD value of 3% is obtained with 3% *trans*-$[RhCl_2(H_2O)_4]^+$, 49% *cis*-$[RhCl_2(H_2O)_4]^+$ and 48% *mer*-$[RhCl_3(H_2O)_3]$. Note that the NRMSD values are only calculated above 210 nm, because the absorption intensity in the UV-vis spectrum below 210 nm is due to excess aqueous

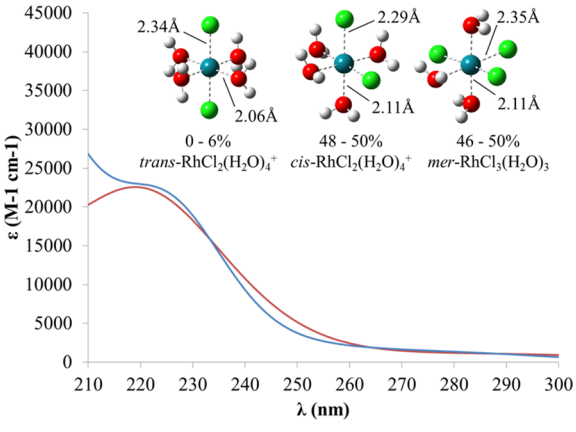

Figure 2. Experimental spectrum of the Rh(III) chloride sample dissolved in pure water (blue) overlaid with the LC-wPBE/aug-cc-pVTZ (red) predicted UV-vis spectrum that results from fitting the individual absorption contributions of all optimized Rh chloride species. The relative concentration ranges span all fits whose NRMSD values were below a tolerance threshold of 5%, relative to the experiment. The optimized structures of the major species along with their key bond lengths are presented.

dx.doi.org/10.1021/ic501408r | *Inorg. Chem.* 2014, 53, 12315−12322

chloride, which has a λ_{max} value of 193 nm and has not been modeled in the TD-DFT simulations.[37] From a thermodynamic perspective, prior work and the calculated free energies for chloride substitution determined here indicate a strong driving force for chloride substitution (see Table 4). However, in pure water, there is little excess chloride, and, thus, it is believed that the speciation in the 0 M HCl solution is unchanged, relative to the original sample.

Table 4. Solution-Phase B3LYP/cc-pVDZ Predicted ΔG_{rxn} of Chloride Complexation Reactions in Aqueous Solution

chemical reaction	ΔG_{rxn} [kcal/mol]
$[Rh(H_2O)_6]^{3+} + Cl^- \rightarrow RhCl(H_2O)_5]^{2+} + H_2O$	−32.9
$[RhCl(H_2O)_5]^{2+} + Cl^- \rightarrow$ *cis*-$[RhCl_2(H_2O)_4]^+ + H_2O$	−4.2
$[RhCl(H_2O)_5]^{2+} + Cl^- \rightarrow$ *trans*-$[RhCl_2(H_2O)_4]^+ + H_2O$	−2.2
cis-$[RhCl_2(H_2O)_4]^+ + Cl^- \rightarrow$ *fac*-$[RhCl_3(H_2O)_3] + H_2O$	−13.1
trans-$[RhCl_2(H_2O)_4]^+ + Cl^- \rightarrow$ *fac*-$[RhCl_3(H_2O)_3] + H_2O$	−14.0
cis-$[RhCl_2(H_2O)_4]^+ + Cl^- \rightarrow$ *mer*-$[RhCl_3(H_2O)_3] + H_2O$	−12.6
trans-$[RhCl_2(H_2O)_4]^+ + Cl^- \rightarrow$ *mer*-$[RhCl_3(H_2O)_3] + H_2O$	−13.5
fac-$[RhCl_3(H_2O)_3] + Cl^- \rightarrow$ *cis*-$[RhCl_4(H_2O)_2]^- + H_2O$	−7.4
fac-$[RhCl_3(H_2O)_3] + Cl^- \rightarrow$ *trans*-$[RhCl_4(H_2O)_2]^- + H_2O$	−6.2
mer-$[RhCl_3(H_2O)_3] + Cl^- \rightarrow$ *cis*-$[RhCl_4(H_2O)_2]^- + H_2O$	−7.9
mer-$[RhCl_3(H_2O)_3] + Cl^- \rightarrow$ *trans*-$[RhCl_4(H_2O)_2]^- + H_2O$	−6.7
cis-$[RhCl_4(H_2O)_2]^- + Cl^- \rightarrow [RhCl_5(H_2O)]^{2-} + H_2O$	−4.8
trans-$[RhCl_4(H_2O)_2]^- + Cl^- \rightarrow [RhCl_5(H_2O)]^{2-} + H_2O$	−6.0
$[RhCl_5(H_2O)]^{2-} + Cl^- \rightarrow [RhCl_6]^{3-} + H_2O$	1.9
$[RhCl_3(H_2O)_3] + [RhCl_3(H_2O)_3] + 3Cl^- \rightarrow [Rh_2Cl_9]^{3-} + 6H_2O$	−4.5
$[RhCl_3(H_2O)_3] + [RhCl_4(H_2O)_2]^- + 2Cl^- \rightarrow [Rh_2Cl_9]^{3-} + 5H_2O$	0.8
$[RhCl_4(H_2O)_2]^- + [RhCl_4(H_2O)_2]^- + Cl^- \rightarrow [Rh_2Cl_9]^{3-} + 4H_2O$	6.0
$[RhCl_4(H_2O)_2]^- + [RhCl_5(H_2O)]^{2-} \rightarrow [Rh_2Cl_9]^{3-} + 3H_2O$	6.5
$[RhCl_5(H_2O)]^{2-} + [RhCl_3(H_2O)_3] + Cl^- \rightarrow [Rh_2Cl_9]^{3-} + 4H_2O$	1.2
$[RhCl_3(H_2O)_3] + [RhCl_6]^{3-} \rightarrow [Rh_2Cl_9]^{3-} + 3H_2O$	−0.7

Speciation of Aqueous Rh(III) under Varying Chloride Concentration. As reported in Table 4, the addition of chloride to the dichlorido and trichlorido species believed to be present in upon dissolution of the sample should be exergonic until the formation of the hexachlorido species. This agrees qualitatively with the experimental free energies of reaction obtained from kinetic studies performed at elevated temperatures.[13−17] The theoretical values at 298 K are 5−10 kcal/mol higher than that obtained in the range of 303−318 K. As chloride is added, the ΔG_{rxn} becomes systematically less favorable, with the formation of the $[RhCl_5(H_2O)]^{2-}$ species from $[RhCl_4(H_2O)_2]^-$ having a free energy of only ca. −5 kcal/mol. Therefore, we expect that the highly chloridated species should form only at high chloride concentration. Under the equilibration conditions, oligomers of Rh chloride can also be produced and thus the competitive reactions of the various chloridated species to form the dimer $[Rh_2Cl_9]^{3-}$ were also investigated. As seen in Table 5, the addition of chloride to $[RhCl_3(H_2O)_3]$ is thermodynamically favored with a ΔG_{rxn} value of −13.5 kcal/mol; however, a secondary pathway that is also favored is the bimolecular reaction of $[RhCl_3(H_2O)_3]$ with itself to form $[Rh_2Cl_9]^{3-}$, having ΔG_{rxn} of −4.5 kcal/mol. Given that we do not know the activation barriers for these processes, it is possible that $[Rh_2Cl_9]^{3-}$ could accumulate over time and be present in solution with the various monomeric chloridated Rh species. As

Table 5. Calculated Speciation of Rh(III) Complexes in Various Concentrations of HCl with Relative Concentrations That Provide a NRMSD Value of ≤ 5%[a]

	Calculated Speciation of Rh(III) Complexes [%]				
Rh(III) species	0 M HCl	0.1 M HCl	0.5 M HCl	1.0 M HCl	2.0 M HCl
cis-$[RhCl_2(H_2O)_4]^+$	48−50	0	0	0	0
trans-$[RhCl_2(H_2O)_4]^+$	0−6	46−50	40−48	0	0
fac-$[RhCl_3(H_2O)_3]$	0	0	32−34	56−60	0
mer-$[RhCl_3(H_2O)_3]$	46−50	50−54	20−26	34−36	0
cis-$[RhCl_4(H_2O)_2]^-$	0	0	0	1−3	78−86
$[RhCl_5(H_2O)]^-$	0	0	0	0	0
$[RhCl_6]^{3-}$	0	0	0	0	0
$[Rh_2Cl_9]^{3-}$	0	0	0	4−6	14−22

[a]For HCl concentrations above 2 M, a fit with a NRMSD ≤ 5% was not found. Fits with minimized NRMSD are presented in Table S5 in the Supporting Information.

the chloride solutions were equilibrated with millimolar concentrations of Rh(III), the formation of polymeric species solution is not unreasonable; however, we note that preparation of these species often employs large stabilizing ligands (e.g., triethyl phosphine) in the remainder of the coordination sphere of Rh(III).[9−11] The formation of $[Rh_2Cl_9]^{3-}$ is also predicted from the reaction of $[RhCl_6]^{3-}$ with $[RhCl_3(H_2O)_3]$; however, this pathway is less likely in solution, as it would require significant concentrations of both the hexachlorido and trichlorido species, and the density functional theory (DFT) results indicate that the formation of the hexachlorido complex is thermodynamically unfavorable. Thus, based on the thermodynamic analysis of the different chloride addition and bimolecular reactions outlined in Table 4, DFT predicts that, as the chloride concentration increases, more substituted chloride species should form with the potential for dimeric $[Rh_2Cl_9]^{3-}$ being present after the formation of the trichlorido complex $[RhCl_3(H_2O)_3]$.

Using the calculated UV-vis absorption spectra of individual $[RhCl_x(H_2O)_{6-x}]^{3-x}$, the experimental spectra were fit to determine the relative concentrations of every complex under different HCl concentrations. As seen in Figure 3, the width of the LMCT peak broadens even at an HCl concentration of 0.1 M, indicating a change in the speciation that is described by the linear combination of TD-DFT excitations of both $[RhCl_2(H_2O)_4]^+$ and $[RhCl_3(H_2O)_3]$ species (see Table 5). The TD-DFT spectra with an NRMSD value of ≤5% have relative concentrations of 46%−50% for *trans*-$[RhCl_2(H_2O)_4]^+$ and 50%−54% for *mer*-$[RhCl_3(H_2O)_3]$. This is also supported by CZE data, as a neutral species is observed (see Table S6 in the Supporting Information). It is interesting to note that in the added HCl medium the trans isomer of $[RhCl_2(H_2O)_4]^+$ predominates, while the cis isomer was prevalent in the original dissolution of the sample in pure water. While we do not have a ready explanation for this observation, we observe only a minimal energy difference between the two isomers, with the cis form being preferred for formation from the $[RhCl(H_2O)_5]^{2+}$ species. However, the calculated computed free energies for chloride addition are somewhat larger than that observed experimentally (albeit at higher temperatures). Thus, it is possible that the complex equilibria that results when excess chloride is present will involve not only the chloride addition reactions, but also some extent of dissociation

dx.doi.org/10.1021/ic501408r | Inorg. Chem. 2014, 53, 12315−12322

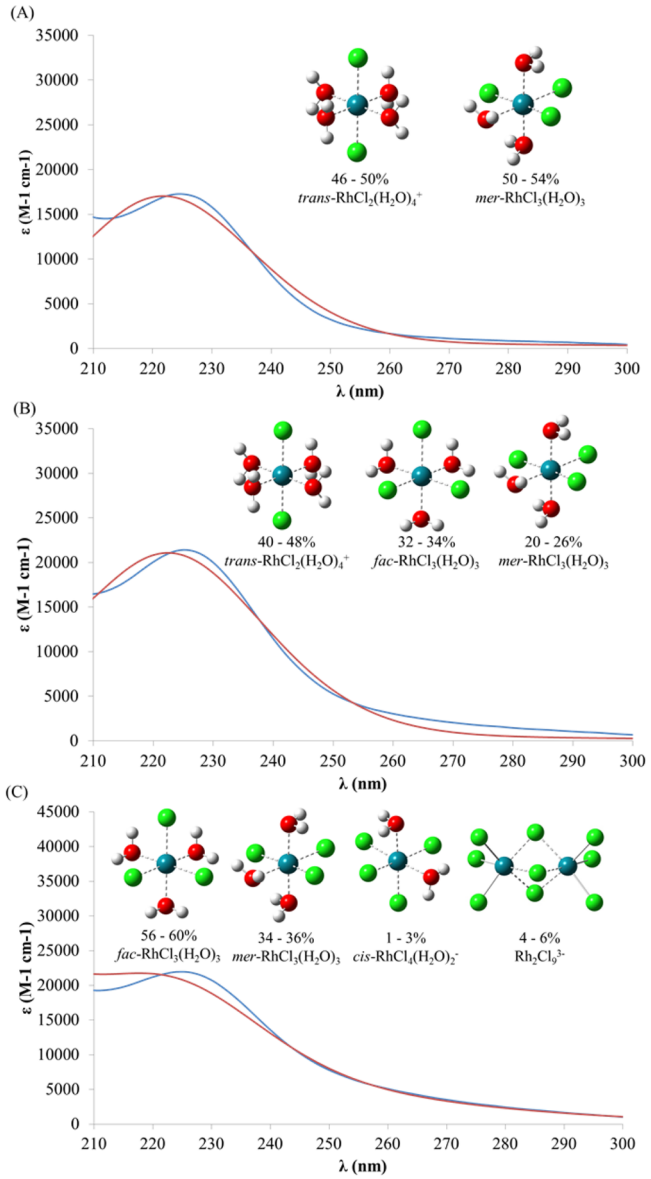

Figure 3. Experimental spectrum of the dissolved Rh chloride sample in (A) 0.1 M HCl, (B) 0.5 M HCl, and (C) 1.0 M HCl (blue) overlaid with the predicted LC-wPBE/aug-cc-pVTZ UV−vis spectrum (red) that results from fitting the individual absorption contributions of all optimized Rh chlorido species. The relative concentration ranges span all fits whose NRMSD values were below a tolerance threshold of 5%, relative to the experiment.

reactions of the trichloride species that favor the trans isomer. Increasing the concentration to 0.5 M reveals further broadening of the absorption band and a 1 nm shift in the peak position. The best fit to experiment results from a mixture of the absorption spectra of *trans*-$[RhCl_2(H_2O)]_4$ (40%−48%), *fac*-$[RhCl_3(H_2O)_3]$ (32%−34%), and *mer*-$[RhCl_3(H_2O)_3]$ (20%−26%). Data from CZE data indicates the presence of at least the neutral species in 0.5 M HCl. The dominant species in 1.0 M HCl is predicted to be the $[RhCl_3(H_2O)_3]$ with a small concentrations of $[RhCl_4(H_2O)_2]^-$ and $[Rh_2Cl_9]^{3-}$. Two species are observed in 1.0 M HCl solution based on the CZE data, one neutral and the other negatively charged (see Table S5 in the Supporting Information).

Determination of the speciation in solution using TD-DFT becomes difficult as the concentration of chloride reaches 2 M. The NRMSD for each fit is ∼10% for each sample above 2 M HCl, which suggests that either a more-complex solution is formed that contains an unknown species, or that the change in the bulk solution properties (ionic strength and dielectric constant) begin to alter the experimental spectrum. When the chloride concentration reaches 6 M the fitted TD-DFT spectrum would indicate that the absorbance associated with $[Rh_2Cl_9]^{3-}$ begin to dominate the spectrum, which reproduces the experimental observation that the entire high-energy band is red-shifted to a value in the range of 250−260 nm (see Figure S2 and Table S3 in the Supporting Information). Data from CZE for the solutions for 2 M HCl and above all indicate the presence of two distinct species in solution, with charges of −2 and −3. This agrees well with predicted speciation determined through TD-DFT fitting in that only two species are seen to dominate in solution where the concentration of HCl is ≥2 M. It is important to note that the hexachlorido complex is not seen in the range of 0−12 M HCl. This is also consistent with the calculated thermodynamic data from both literature and the calculated thermodynamic data presented in this work.[14]

CONCLUSIONS

The speciation of Rh(III) in hydrochloric and nitric acid solutions has been investigated using experimental (UV-vis, CZE) and theoretical (thermodynamic, TD-DFT) techniques. The evidence presented indicate that, in HCl solutions, Rh(III) exists as a mixture of species specifically $[RhCl_x(H_2O)_y]^{3-x}$ (x = 0−6; $y = 6 - x$) and $[Rh_2Cl_9]^{3-}$. The $[RhCl_6]^{3-}$ species was not observed in this study, agreeing with data reported in the literature showing the substitution of the sixth chloride as nonspontaneous at room temperature.[14] As the concentration of HCl increases, increased chloride coordination is observed with Rh(III) and an apparent red shift occurs for both the LMCT and d−d bands of the UV-vis spectra. This trend is supported by the theoretical free energies of chloride addition and CZE data. In contrast, the speciation of Rh(III) in HNO_3 is invariant to the concentration of HNO_3. The UV-vis spectra for Rh(III) in 0−12 M HNO_3 show a single peak with a λ_{max} of 202 nm; in agreement with the simulated TD-DFT spectrum of $[Rh(NO_3)_3]$. The complex speciation of Rh(III) in a chloride medium, relative to nitrate, is likely due to a combination of factors, including smaller binding energies of chloride for substitution beyond $[RhCl_3(H_2O)_3]$ and a more diverse coordination environment caused by the monodentate nature of chloride, relative to the thermodynamically preferred bidentate coordination mode of nitrate. In combination, these data help to clarify and assess the speciation of Rh(III) in acidic media relevant to separations and purification of this precious metal from spent fuel raffinates. The utilization of modern computational methods in combination with experimental techniques also points to a general protocol that can be successfully pursued to determine speciation of precious metals in acidic media.

ASSOCIATED CONTENT

Supporting Information

This material is available free of charge via the Internet at http://pubs.acs.org.

AUTHOR INFORMATION

Corresponding Authors

*E-mail: nawall@wsu.edu (N. A. Wall).
*E-mail: auclark@wsu.edu (A. E. Clark).

Notes

The authors declare no competing financial interest.

■ ACKNOWLEDGMENTS

This work was supported by a grant from the U.S. Department of Energy Nuclear Energy University Program (NEUP) (No. MS-FC-11-3095). A portion of the computational studies were performed using EMSL, a national scientific user facility sponsored by the Department of Energy's Office of Biological and Environmental Research and located at Pacific Northwest National Laboratory.

■ REFERENCES

(1) Kolarik, Z.; Renard, E. V. *Plat. Met. Rev.* **2003**, *47*, 74−87.
(2) Kolarik, Z.; Renard, E. V. *Plat. Met. Rev.* **2005**, *49*, 79−90.
(3) International Atomic Energy Agency. *Technical Reports Series*; International Atomic Energy Agency (IAEA): Vienna, Austria, 1989.
(4) Smith, F. J.; McDuffie, H. F. *Sep. Sci. Technol.* **1981**, *16*, 1071−1079.
(5) Naito, K.; Matsui, T.; Tanaka, Y. *J. Nucl. Sci. Technol.* **1986**, *23*, 540−549.
(6) Paiva, A. P.; Malik, P. *J. Radioanal. Nucl. Chem.* **2004**, *261*, 485−496.
(7) Horwitz, E.; Diamond, H.; Martin, K. A. *Solvent Extr. Ion Exch.* **1987**, *5*, 447−470.
(8) Levitin, G.; Schmuckler, G. *React. Funct. Polym.* **2003**, *54*, 149−154.
(9) Cotton, F. A.; Seong-Joo, K.; Mandal, S. K. *Inorg. Chim. Acta* **1993**, *206*, 29−39.
(10) Rai, D.; Sass, B. M.; Moore, D. A. *Inorg. Chem.* **1987**, *26*, 345−349.
(11) Spiro, T. G.; Allerton, S. E.; Renner, J.; Terzis, A.; Bils, R.; Saltman, P. *J. Am. Chem. Soc.* **1966**, *88*, 2721−2726.
(12) Aleksenko, S. S.; Gumenyuk, A. P.; Mushtakova, S. P.; Timerbaev, A. R. *Fresenius' J. Anal. Chem.* **2001**, *370*, 865−871.
(13) Palmer, D. A.; Harris, G. M. *Inorg. Chem.* **1975**, *14*, 1316−1321.
(14) Pavelich, M. J.; Harris, G. M. *Inorg. Chem.* **1973**, *12*, 423−431.
(15) Robb, W.; Harris, G. M. *J. Am. Chem. Soc.* **1965**, *87*, 4472−4476.
(16) Swaminathan, K.; Harris, G. M. *J. Am. Chem. Soc.* **1966**, *88*, 4411−4414.
(17) Robb, W.; de V. Steyn, M. M. *Inorg. Chem.* **1967**, *6*, 616−619.
(18) Caminiti, R.; Atzei, D.; Cucca, P.; Anedda, A.; Bongiovanni, G. *J. Phys. Chem.* **1986**, *90*, 238−243.
(19) Cramer, C. J.; Truhlar, D. G. *Phys. Chem. Chem. Phys.* **2009**, *11*, 10757−10816.
(20) Niu, S.; Hall, M. B. *Chem. Rev.* **2000**, *100*, 353−406.
(21) Valiev, M.; Bylaska, E. J.; Govind, N.; Kowalski, K.; Straatsma, T. P.; Van Dam, H. J. J.; Wang, D.; Nieplocha, J.; Apra, E.; Windus, T. L. *Comput. Phys. Commun.* **2010**, *181*, 1477−1489.
(22) Braun-Sand, S. B.; Wiest, O. *J. Phys. Chem. A* **2003**, *107*, 285−291.
(23) Peterson, K. A.; Figgen, D.; Dolg, M.; Stoll, H. *J. Chem. Phys.* **2007**, *126*, 124101.
(24) Dunning, T. H., Jr. *J. Chem. Phys.* **1989**, *90*, 1007.
(25) Woon, D. E.; Dunning, T. H., Jr. *J. Chem. Phys.* **1993**, *99*, 3730.
(26) Frisch, M. J.; Trucks, G. W.; Schlegel, H. B.; Scuseria, G. E.; Robb, M. A.; Cheeseman, J. R.; Scalmani, G.; Barone, V.; Mennucci, B.; Petersson, G. A. et al.*Gaussian09*; Gaussian, Inc.: Wallingford, CT, 2009; p 115.
(27) Asthagiri, D.; Pratt, L. R.; Kress, J. D. *Phys. Rev. E* **2003**, *68*, 041505.
(28) Vicek, A.; Zalis, S. *Coord. Chem. Rev.* **2007**, *251*, 258−287.
(29) Tawada, Y.; Tsuneda, T.; Yanagisawa, S.; Yanai, T.; Hirao, K. *J. Chem. Phys.* **2004**, *120*, 8425.
(30) Stephens, P. J.; Harada, N. *Chirality* **2010**, *22*, 229−233.
(31) Belyaev, A. V.; Fedotov, M. A.; Khranenko, S. P.; Emel'yanov, V. A. *Russ. J. Coord. Chem.* **2001**, *27*, 855−864.
(32) Critchlow, P. B.; Robinson, S. D. *Inorg. Chem.* **1978**, *17*, 1896−1901.
(33) Lever, A. B. P.; Mantovani, E.; Ramaswamy, B. S. *Can. J. Chem.* **1971**, *49*, 1957−1964.
(34) Wolsey, W. C.; Reynolds, C. A.; Kleinberg, J. *Inorg. Chem.* **1963**, *2*, 463−468.
(35) Blasius, E.; Preetz, W. *Chromatogr. Rev.* **1964**, *6*, 191−213.
(36) Brauer, G. *Handbook of Preparative Inorganic Chemistry*; Academic Press: New York, 1963.
(37) Higashi, N.; Ozaki, Y. *Appl. Spectrosc.* **2004**, *58*, 910−916.